NASA/TM–2019-220250

Calibration of a Structural Finite Element Model for a Representative Inflatable Space Structure Utilizing Probabilistic Methods and Surrogate Models

Karen H. Lyle and Thomas C. Jones
Langley Research Center, Hampton, Virginia

February 2019

NASA STI Program . . . in Profile

Since its founding, NASA has been dedicated to the advancement of aeronautics and space science. The NASA scientific and technical information (STI) program plays a key part in helping NASA maintain this important role.

The NASA STI program operates under the auspices of the Agency Chief Information Officer. It collects, organizes, provides for archiving, and disseminates NASA's STI. The NASA STI program provides access to the NTRS Registered and its public interface, the NASA Technical Reports Server, thus providing one of the largest collections of aeronautical and space science STI in the world. Results are published in both non-NASA channels and by NASA in the NASA STI Report Series, which includes the following report types:

- TECHNICAL PUBLICATION. Reports of completed research or a major significant phase of research that present the results of NASA Programs and include extensive data or theoretical analysis. Includes compilations of significant scientific and technical data and information deemed to be of continuing reference value. NASA counter-part of peer-reviewed formal professional papers but has less stringent limitations on manuscript length and extent of graphic presentations.

- TECHNICAL MEMORANDUM. Scientific and technical findings that are preliminary or of specialized interest, e.g., quick release reports, working papers, and bibliographies that contain minimal annotation. Does not contain extensive analysis.

- CONTRACTOR REPORT. Scientific and technical findings by NASA-sponsored contractors and grantees.

- CONFERENCE PUBLICATION. Collected papers from scientific and technical conferences, symposia, seminars, or other meetings sponsored or co-sponsored by NASA.

- SPECIAL PUBLICATION. Scientific, technical, or historical information from NASA programs, projects, and missions, often concerned with subjects having substantial public interest.

- TECHNICAL TRANSLATION. English-language translations of foreign scientific and technical material pertinent to NASA's mission.

Specialized services also include organizing and publishing research results, distributing specialized research announcements and feeds, providing information desk and personal search support, and enabling data exchange services.

For more information about the NASA STI program, see the following:

- Access the NASA STI program home page at http://www.sti.nasa.gov

- E-mail your question to help@sti.nasa.gov

- Phone the NASA STI Information Desk at 757-864-9658

- Write to:
  NASA STI Information Desk
  Mail Stop 148
  NASA Langley Research Center
  Hampton, VA 23681-2199

NASA/TM–2019-220250

Calibration of a Structural Finite Element Model for a Representative Inflatable Space Structure Utilizing Probabilistic Methods and Surrogate Models

Karen H. Lyle and Thomas C. Jones
Langley Research Center, Hampton, Virginia

National Aeronautics and
Space Administration

Langley Research Center
Hampton, Virginia 23681-2199

February 2019

Available from:

NASA STI Program / Mail Stop 148
NASA Langley Research Center
Hampton, VA 23681-2199
Fax: 757-864-6500

Abstract

A structural finite element model representing a novel inflatable airlock concept has been calibrated using full-scale test data. The concept, denoted as the Non-Axisymmetric Inflatable Pressure Structure (NAIPS), was developed under NASA's Minimalistic Advanced Softgoods Hatch (MASH) Program. The current studies extended previous numerical efforts by incorporating the midbody section of the NAIPS to the dome section and calibrating the model with test data using a process that included surrogate models. Brief overviews of the finite element model and calibration process are provided. The completion of the calibration process provided a model that adequately replicated the test data. The successful demonstration of calibration of a finite element model representing an inflatable habitat provides confidence in the ability to use numerical simulations and associated surrogate models to support design and certification of inflatable space habitats.

Introduction

Robust inflatable space structures are in demand for a number of applications due to their efficient packaging and light weight versus rigid shell structures. Traditionally, evaluations of design concepts and subsequent certifications have been performed through testing because of the limited analysis capability for softgoods structures. However, recent advances in simulation capability and computational speed have enabled finite element model (FEM) simulations of a wide range of aerospace applications. Examples where numerical simulations were utilized in soft-goods applications include: inflatable habitats such as the Bigelow Expandable Activity Module (BEAM)[1,2]; atmospheric decelerators such as the Hypersonic Inflatable Aerodynamic Decelerator (HIAD)[3,4]; attenuation systems such as the Orion Crew Module Airbag Landing System[5,6]; and aerospace recovery systems[7].

Complementary to the advances in structural computational capabilities has been the implementation of probabilistic methods and establishment of standards for verification and validation of numerical simulations. Several technical societies and agencies are developing standards for documenting the uncertainty of responses to variations in input parameters[8-10]. For probabilistic analyses, sophisticated methods may be required to optimally use the results from a relatively small number of simulations. The choice of method is dependent on the number of uncertain parameters, the number and types of responses, the simulation execution time, and the physics of the application. Examples of aerospace applications incorporating probabilistic methods are provided in Refs. 11 and 12.

As NASA continues to explore the use of inflatables for a variety of applications, development of a certification plan for human-rated inflatable space structure is critical[13]. Robust analysis techniques for inflatables need to be explored and verified so they can be incorporated

into the design and certification of future softgoods structures. A novel inflatable airlock concept, called the Non-Axisymmetric Inflatable Pressure Structure (NAIPS) under the Minimalistic Advanced Softgoods Hatch (MASH) Program[14,15], is the application focus of this report, see Figure 1. The NAIPS structural analysis problem represents many design challenges, including: 1) the lack of formal design approaches to address such softgoods hatch concepts; and 2) modeling the behavior of complex structural responses that include uncertainty in softgoods material properties and transfer of loads through multiple paths and different softgoods elements. Fortunately, the detailed computational tools needed to analyze the structural response of such systems are becoming sufficiently mature to adequately model the response of these complex structures. Additionally, it is now feasible to complete the numerous nonlinear transient dynamic simulations that are critical to support verification of the design in a reasonable amount of time. For cases where hundreds of FEM evaluations may be needed, time constraints may necessitate the use of surrogate models. Once the calibration parameters of a design are determined using surrogate model results, the finite element model can be executed to verify the calibration parameters or design.

Previous studies, focusing on end-state loads in the NAIPS inflatable habitat dome section, were reported in Refs. [16 and 17]. The current studies extend the previous results by: integrating the midbody section with the previously studied dome section; and calibrating the model with a process that included surrogate models. Responses of interest focused on those that were measured during the testing, namely, cord loads and fabric strains. Brief descriptions of the NAIPS module and testing, the finite element model, and the model calibration process are provided, followed by a discussion of the results. Within the discussion of the results, model calibration parameters and the corresponding comparison of calibrated model results with an expanded set of test data are provided along with parameter sensitivities. Finally, concluding remarks provide general comments about the approaches and findings.

Description of NAIPS Inflatable Module and Testing

The NAIPS is an inflatable airlock structure that consists of a high-specific strength Vectran fabric shell constrained by a series of braided Vectran cords, see Figure 1, and is sized to provide adequate room for two astronauts to don and doff their space suits, prior to exiting the airlock. The novel shape of the NAIPS is enforced by the position and sizing of the cordage. The shape provides areas of low hoop stress in the lobes at each end dome and along the midbody, which allow the integration of a linear soft hatch, similar in operation to a zipper. This feature significantly reduces the total mass of the airlock by eliminating the large metallic EVA hatch that would otherwise be required. The internal pressure is carried primarily by the cords, which are loaded via the underlying fabric shell. This design approach is also highly scalable to larger applications including a space hangar or inflatable logistics bay for future outposts, see Figure 2, where a large opening is required and where a typical rigid hatch would be mass prohibitive.

A full-scale test article of the NAIPS was fabricated and pressure tested at NASA LaRC[15] in 2016 and was instrumented with load cells on 50% of the meridional (or radial) cords, see Figure 3, in addition to full-field strain measurements being taken by 8 photogrammetry camera systems, see Figure 4. Mechanical property tests were also performed prior to the full-scale test on fabric and cord specimens to obtain their load-strain properties. The load-strain behavior of these softgoods is highly non-linear as woven fabric and braided cords undergo large displacements at the onset of loading, due to decrimping and untwisting of the yarns, in addition to material strain. The load-strain behavior also changes as the materials are cyclically loaded through the pressurization/depressurization of the airlock. Additional specimen testing was performed after the full-scale test to acquire load-strain curves for specimens that had undergone representative cyclical loading to better represent the test pressurizations performed on the full-scale article. This material data for the fabric and cordage was used in the subsequent FEM analyses and the results of those analyses were compared to the load and strain readings measured during the final pressure test to burst of the NAIPS test article.

Description of Analyses

The numerical model and probabilistic methods used in this publication relied on lessons-learned from earlier efforts focusing on analysis of the dome section of the NAIPS[16, 17]. These prior publications contain detailed information about the modeling approach, therefore only a brief summary of that information is provided here. These previous studies supported the development of this model by: improving the numerical stability; shortening the execution time; and increasing confidence in the probabilistic methods and surrogate models used in this work.

Finite Element Model

An existing explicit, dynamic finite element model of the full-scale test article, see Figure 5, was simplified by extracting a quarter symmetry section, see Figure 6a. The FEM for these studies contained 14,175 nodes. The orthotropic fabric was represented by 12,880 fully-integrated shell elements and the network of cords by 1,236 beam elements.

At the start of the simulations the article is deflated, see Figure 6a. The symmetry boundary conditions enabling execution of a quarter model are also specified. In the test article, the radial cords are fabricated shorter than the underlying fabric, to induce the formation of the low-stress lobes and enable transfer of much of the load from the fabric to the radial cords. Likewise, the axial cords are also shorter in the physical article, where the axial cordage loops off-load much of the axial load in the midbody fabric. To improve numerical stability in the FEM simulations, the radial and axial cords were initially sized to the flattened state and then shrunk during inflation using a thermal contraction of a specified set of beam elements; these are referred to herein as thermal elements, see Figure 6b. The thermal elements at each end of the radial cords were attached to the axial cord that formed a loop on the top and bottom of each

end dome. The axial cord thermal elements were located near the center of the midbody.

The normalized profiles for both the pressure (inflation) and thermal loads are shown in Figure 7. The pressure load is applied to the fabric inner surface and linearly increased from zero to a prescribed value over the time range from 0 to 0.3 seconds. The primary goal of the history profile for the pressure load was to enable "inflation" while also minimizing execution time and mitigating unwanted transient dynamic behavior. The pressure loading profile is not intended to replicate the actual inflation time of the airlock. It should be noted that the material damping was increased during the initial pressure loading to minimize transient dynamic behavior. Concurrently, a linear temperature decrease is applied to the thermal elements from 0 to 0.15 seconds. The simulations are executed until 0.4 s to allow the loads to reach equilibrium.

Contact implementations are crucial to these simulations by enabling transfer of loads between the softgoods components. All of the contacts are penalty-based, where the friction and penalty-force stiffness scale factors can be varied. Prior modeling experience showed that modifications to the contact parameters were required for numerical stability of the simulations. Unfortunately, it was not possible to mitigate all numerical stability issues with the addition of the midbody to the dome.

The numerical simulations were executed in LS-Dyna[18], a commercial, general-purpose, nonlinear, transient-dynamic, finite element code. The fabric and cord materials are represented by nonlinear stress-strain curves derived from test data. A material model that was specifically formulated for fabric was selected to represent the behavior of the woven material. The braided cords were represented by a cable material model formulation. The computational time to process the 0.4-second responses was approximately 3 to 4 hours using 8 processors. Unlike most applications using an explicit, transient-dynamic analysis, only the end-state results, and not the time-varying responses, were of interest to represent the quasi-static inflation of the test article.

Calibration Process

In general, sensitivity analyses and model calibration can be conducted using either finite element simulations or surrogate model approximations. Due to time constraints and issues with numerical stability, the model for this application was calibrated using surrogate models generated from a set of FEM simulations. The calibration process was conducted using probabilistic analyses tools available in the commercial optimization code LSOpt[19], see flow chart in Figure 8. Results from the calibration process are dependent on: (#1) parameter setup by the selection of the uncertain parameters and bound, (#2) the parameter sampling approach, (#3) the solver or simulation code, (#4) the surrogate model, (#5) the sensitivity metric, and (#6) the optimization methods which includes objectives and constraints. Since surrogate models were used, the final step of the calibration process requires execution of the finite element model to verify the calibration results (#7). Each of these topics will be discussed below.

A total of 8 parameters were considered in the analyses, see Table I. Material properties

of the four different softgoods components in the model were varied through multiplicative factors on the ordinate of each of the load-strain curves: the radial cord (F_{RC}), the axial cord (F_{AC}), the dome fabric (F_{DF}), and the midbody fabric (F_{MF}). The coefficients of thermal expansion, α_{RC} and α_{AC}, applied to the radial cord and axial cord thermal elements, respectively, were varied to enable changes in the cord lengths. For the calibration process, α_{RC} and α_{AC} are independent input parameters and the radial cord length (L_{RC}) and the axial cord length (L_{AC}) are constrained responses. The final two parameters are the contact frictions, μ_D and μ_M, applied to the dome-fabric-to-radial-cords and the midbody-fabric-to-axial-cords, respectively. The parameter bounds for the FEM simulations were based on engineering judgment. The scaling bounds for material property incorporated insight from the sensitivity studies in Refs. [16 and 17], as well as review of the baseline material property testing.

Matlab[20] scripts were utilized to control parameter sampling, execution of the LS-Dyna simulations, and preliminary data reduction. Although there are many techniques that can create adequate sampling of the parameter space for a probabilistic analysis, Halton-Leap deterministic sampling[21] was chosen for this study. The Halton-Leap method creates uncorrelated, multi-dimensional, uniformly distributed values between 0 and 1, which are then converted to engineering values. For model calibration, four representative responses were selected, namely: radial cord load ($P_{RC}{}^5$); axial cord load ($P_{AC}{}^2$); dome warp strain ($\varepsilon_{DF}{}^1$); and midbody warp strain ($\varepsilon_{MF}{}^4$), see Figure 9. The surrogate model calibration was performed at the operational inflation pressure of 15 psi.

Two surrogate model methods have been explored for this application: a response surface method[22] based on the linear and the cross terms [but not the quadratic terms] ($SM_1{}^+$); and the Kriging method (SM_3)[23]. A surrogate model describes the relationship between the sample input parameters and one of the outputs of interest, which include cord loads and fabric strains. To determine the adequacy of the surrogate models, the RMS error of the surrogates versus the FEM simulations were computed, see Table II. The errors for both surrogate models are small (within a few percent). As with all studies, the project's required accuracy or adequacy needs are critical to determining which approach is best suited to the application.

There are a number of methods for computing sensitivities and ranking variables. These include local gradient-based methods[24], and global techniques[25,26]. Results for two global sensitivity methods are provided. From previous experiences with modeling inflated fabric structures, the global correlation method, derived directly from simulation results, has proven to be acceptable for understanding the importance of variables, even under large deformations and nonlinear stress-strain behaviors[12]. In contrast, the Sobol[26] sensitivity method relies on a large number of response samples (i.e., thousands) to compute the variance. It is possible to compute 10,000 responses in minutes using a surrogate model, where 10,000 FEM simulations would take orders of magnitude longer.

The FEM was calibrated to the test data through an optimization process that included

objective functions and constraints, see Table III. Specifically, the objective functions' targets are derived from full-scale experimental data at the 15-psi test point[15]. In addition, constraints are applied to the cord lengths (L_{RC} and L_{AC}). A primary purpose of these studies is not only to calibrate this model, but to gain experience and insight into multiple methods available for optimization. Thus, two common optimization methods available in LS-Opt, namely simulated annealing (SA) and genetic algorithm (GA), were exercised. Simulated annealing is analogous to the metallurgical annealing process, where the desire is to minimize the objective function, the corresponding analog to the temperature. The genetic algorithm is intended to replicate the nature process of survival, where the objective function is an analog to the fitness of an individual. Both optimization methods find an approximate global solution. Both LS-Opt optimizer options were then allowed to refine the solution by switching to the gradient-based Leapfrog method. With two surrogate models and two optimization methods, a matrix of four calibration solutions was computed, see Table IV.

The last step in the calibration process was surrogate model verification. Specifically, comparing the responses from the surrogate models at the calibration parameters to the corresponding finite element simulation results.

Discussion of Results

The results will focus on four areas. First, the parameter sensitivities will be provided, followed by results of the calibration process incorporating surrogate models. Third, the calibration results based on the surrogate models will be verified by comparison with simulations executed at the calibration solutions. Finally, an expanded set of responses will be computed at multiple pressures to compare with full-scale test data.

The Halton-Leap method produces an uncorrelated, deterministic parameter set. Ideally, each parameter is perfectly correlated with itself ($|R| = 1$) and uncorrelated with the other parameters ($|R| = 0$). A review of results for the 100 attempted simulations showed that 78 were numerically stable for the duration of the 0.4 s of execution. When only the 78 numerically stable simulations were retained, the $|R|$ values for F_{RC} and F_{AC}, show a slight interdependence ($|R| = 0.2$). These results highlight ways that numerically unstable simulations can impact a set of results generated from a seemingly independent parameter set. The level of interdependence provides insight about parameter interactions. Fortunately, the level of interdependence for these simulations is not sufficient to impact the calibration results.

Sensitivity results

Sensitivity results are provided in Figure 10, for both global correlation and Sobol coefficients. By noting the similarities and differences, these results highlight the insights that can be gleaned from exercising multiple sensitivity methods. It is important to remember that because these are global measures, the sensitivities are dependent on the parameter ranges.

Sobol coefficients were computed for both of the surrogate models. The cord lengths, L_{RC} and L_{AC} are nearly perfectly correlated (i.e., $|R| > 0.99$) to the respective thermal coefficients, α_{RC} and α_{AC}, as expected due to their dependence, and will not be shown. There appears to be mixed results as far as importance of the various parameters on the radial cord loads (P_{RC}^5). Two of the metrics indicate that the axial cord load (P_{AC}^2) variation is dominated by the axial cord length (L_{RC}) through the axial cord thermal coefficient (α_{AC}). Both of the fabric strain (ε_{DF}^1 and ε_{MF}^4) variations are nearly completely dependent on the corresponding factor applied to the load-strain curves (F_{DF} and F_{MF}).

Calibration of finite element models

Initial trial calibrations indicated that it was not possible to attain the results produced by the NAIPS test when limiting the bounds to those used for the initial simulation bounds, as provided in Table I. Specifically, these preliminary calibration solutions would reach at least one of the parameter's bounds before the calibration targets were met. Following the review of the preliminary calibration results, it was decided to expand the parameter bounds beyond those used for the initial simulations, see Table V. The revised ranges used for the calibration process that fall outside the simulation ranges are highlighted in bold. Thus, the calibration optimization process extrapolated the surrogate models beyond the simulation bounds.

The calibration parameters provided in Table V are for each of the solutions denoted in Table IV. Looking closely at these results, it is important to note similarities and differences across the four solutions. Similarities provide confidence in the behavior, while differences can highlight deficiencies in the process or lack of parameter importance.

A comparison of the load vs. strain behavior taken from cordage and fabric specimen testing is compared to the calculated scaled load vs. strain behavior from the four solutions in Figures 11 and 12. The cord factors (F_{RC} and F_{AC}) in Table V, show considerable scatter between the four curves used as input for the calibration solutions, see Figure 11. By contrast, there is small scatter in the calibration solutions for the fabrics warp and weft curves, Figure 12. Although the calibration was based on only the warp direction strains, the same factor was applied to both the warp and corresponding weft directions. The measured weft strains were very small and sometimes negative, indicating a folding of the fabric. It should be noted that all of the fabric calibration curves are substantially stiffer than the measured curves, which helped determine that the test fixture and methodology were inadequate. Biaxial fabric tests are being investigated to provide a better test data set for future comparison. The sensitivity results showed that the calibration responses were essentially independent of the friction, thus the large scatter in the friction values across the four solutions is not surprising. With the exception of Solution 3:α_{AC}, the thermal coefficients are relatively consistent across the four solutions, indicating a relatively well-behaved optimization space for the corresponding cord lengths.

Verification of calibrated models

At the conclusion of a calibration process that incorporates surrogate models, it is important to verify the solution by executing the FEM with the calibration parameters. For each of the four solutions, a verification simulation was executed and compared to the surrogate model results, see Table VI. The verification simulations are particularly important for this application, as parameter ranges for the underlying simulations were narrower than those allowed for the calibration process. In general, the surrogate cord loads were higher than the simulations, while the surrogate fabric strains were lower. As a means of quantifying the adequacy of the calibration process, the normalized RMS error for each of the solutions was computed, see the bottom row of Table VI. The RMS error was less than 6% for all solutions. The main distinguishing characteristic is that the Kriging surrogate models (SM_3) used for Solutions 2 and 4 resulted in less error than the Linear+Crossterms surrogate (SM_1^+) used for Solutions 1 and 3. It would be up to the designers and project as to whether the relatively simple SM_1^+ or the more complex approach of SM_3 surrogate model would be better for the application.

The results for the verification simulations at 15 psi were expanded from the 4 used in the calibration process to the 8 fabric strains and 6 radial cord responses shown in Figure 13. Since, no test data were acquired for the axial cords, the numerical axial cord loads have been compared with hand-calculated analytical upper bounds. For Figure 14a, both the test and analysis show a spatial trend where the maximum radial cord loads are seen at the middle of the quarter dome section (i.e. at approximately the 45-degree lines on the full end domes). The scatter in the test data is substantially greater than the variation produced by the 4 solutions due to probable small length variations in fabrication of the actual cordage. With the exception of Cord 1, the predicted values were within the scatter of the measured values. As no test data were acquired for the axial cord loads, these loads are compared with an analytical upper bound, see Figure 14b. All of the solutions show values less than the upper bound. Moving on to the fabric strains, the results for the 4 solutions are plotted against the test result bounds for three locations on the dome, in Figure 14c. Both test and analysis show a significant decrease in warp strain when going from Lobe 1 to Lobe 3, however, the test shows a trend of leveling off of the strains, while the numerical trends are nearly linear. Finally, the midbody warp strains are compared to bounds for the test data, see Figure 14d. At 15 psi, Solutions 1 and 3, slightly over predict the midbody strains while solutions 2 and 4 remain within the test result bounds.

In general, the variations within the test data and the differences between test and analysis are greater than the differences between the four solutions. For this reason, only results for one solution will be compared with the range of test data from 10 to 23.5 psi in the next section. All of the solutions were considered acceptable from an accuracy perspective. Solution 1 was selected for the extended comparisons, since: the response surface tends to be easier to implement and the associated expressions can also be more straightforward to interpret than

those for methods such as Kriging; Solution 1 could be considered as the worst case bound based on Table VI (although the error is small); and the simulations were numerically stable. However, it is noted that Solutions 2 and 4 using Kriging surrogate models should produce smaller differences between test and analysis.

Test vs Analysis

Comparison of test with calibrated model results for multiple inflation pressures have been provided in Figure 15, where the x-axis corresponds to the test data, while the y-axis corresponds to FEM simulation results. It is not anticipated that simulations will agree perfectly with test data as uncertainty in the test data exists and modeling deficiencies are inherent in the simulations. As a guide for simulation adequacy, +/- 10% and +/- 20% bounds have been included. In Figure 15a for the radial cords, the simulations fall within the +/- 10% bounds with the exception of Cord 1. Preliminary deterministic studies showed that the load in Cord 1 is very sensitive to modelling details at the dome-to-midbody interface. These details would not have been picked up by P_{RC}^5 used for the calibrations. The localized factors affecting Cord 1 loads that were not included in these calibration studies could be part of a follow-on calibration effort. In lieu of data, a simple computation of the axial cord load upper bound was computed, see Figure 15b. The predicted values all fall below that analytical upper bound.

The measured and predicted warp strains in the dome lobes is provided in Figure 15c. The predictions fall within the measured range, except for Lobe 3, as might be expected from results provided in Figure 14c. Finally, the measured midbody fabric strains are compared with the predictions in in Figure 15d. The pressure has a bigger effect on the measured strains than those that are predicted.

As was noted previously, the model used for the calibration effort was extracted from a preliminary full model. Comparisons of the test data with the preliminary model results were provided in Ref. 15. A list of areas that could have contributed to the discrepancy of the test with analysis was included. An appendix has been included with this report that summarizes: the earlier comparisons along with the current calibrated comparisons; and the modeling changes that addressed the earlier concerns and improved the numerical stability.

Concluding Remarks

A structural finite element model representing a novel inflatable airlock concept has been calibrated using full-scale test data. The concept, denoted as the Non-Axisymmetric Inflatable Pressure Structure (NAIPS), was developed under NASA's Minimalistic Advanced Softgoods Hatch (MASH) Program. The current studies extended previous numerical studies by: incorporating the midbody section to the dome section in the finite element model; and calibrating the numerical model using a process that includes surrogate models. Four model calibration solutions were computed from a matrix of two surrogate models and two optimization processes.

The following observations are made:

- The model calibration was enabled by allowing parameters to extrapolate outside the original simulation ranges. The solutions computed using the surrogate models were verified through comparisons with finite element simulation results. The RMS error of the surrogate models for the calibration process was less than 6%. This level of agreement was considered sufficient to continue comparisons of test data with an expanded set of responses.
- The sensitivity results showed that: the radial cord loads are most dependent on the radial cord length (through the radial cord thermal coefficient) with smaller contributions from other parameters; the axial cord loads show an even stronger dependence on axial cord length (through the axial cord thermal coefficient); and the fabric strains were dominated by the factors applied to the fabrics' stress-strain curves.
- The scatter in test data and differences between test and analysis were generally greater than the scatter in responses for the four possible solutions.
- The final comparisons of test to analysis were conducted at 10 to 23.5 psi.
    - Radial cord loads: numerical model replicates spatial trends; 88 % of the responses for Solution 1 were with +/- 10% of the test data.
    - Axial cord loads: No test data was acquired. The numerical responses are less than the upper analytically calculated bound.
    - Dome fabric warp strains: numerical model replicates the spatial trends; 58% of the responses for Solution 1 were with +/- 10%. This low comparison metric is directly related to test-simulation differences for Lobe 3.
    - Midbody fabric warp strains: 75% of the predictions for Solution 1 were within +/- 10% of the measured values.
- Issues yet to be resolved include:
    - Will updated biaxial fabric test results reduce the observed large deviation between the calculated fabric material properties and the tested load vs strain behavior?
    - Can the numerical stability be improved through remeshing, additional contact definition changes?

In summary, the successful demonstration of the calibration of a finite element model representing an inflatable module provides confidence in the ability to use numerical simulations and associated surrogate models to support certification of inflatable space habitats.

Acknowledgements

The authors would like to recognize the contributions of Mr. Alberto Makino (NASA Ames Research Center), who provided the preliminary model and simulation results.

References

1. Lyle, K. H. and Vassilakos, G. J.: Modeling of Global BEAM Structure for Evaluation of MMOD Impacts to Support Development of a Health Monitoring System. NASA/TM-2015-218984. November 2015.
2. Lyle, K. H. and Vassilakos, G. J.: Modeling of Local l BEAM Structure for Evaluation of MMOD Impacts to Support Development of a Health Monitoring System. NASA/TM-2015-218984. November 2015.
3. Lindell, M. C., Hughes, S. J., Dixon, M, and Willey, C. E.: Structural Analysis and Testing of the Inflatable Re-entry Vehicle Experiment (IRVE). Proceedings of the 47th AIAA/ASME/ASCE/AHS/ASC Structures, Structural Dynamics, and Materials Conference, AIAA Paper No. 2006-1699, Newport RI, 1-4 May 2006.
4. Lyle, K. H.: Comparison of Analysis with Test for Static Loading of Two Hypersonic Inflatable Aerodynamic Decelerator Concepts. NASA TM-2015-218778, July 2015.
5. Timmers, R. B.; Hardy, R. C.; and Welch, J. V.: Modeling and Simulation of the Second-Generation Orion Crew Module Air Bag Landing System. Proceeding of the 20th AIAA Aerodynamic Decelerator Systems Technology Conference and Seminar, AIAA Paper No. 2009-2921, Seattle WA, May 4-7, 2009.
6. Tutt, B.; Johnson, R. K.; and Lyle, K.: Development of an Airbag Landing System for the Orion Crew Module. Proceedings of the 10th International LS-Dyna Users Conference, Dearborn MI, June 8-10, 2008.
7. Tutt, B. A.; and Taylor, A. P.: Applications of LS-Dyna to Structural Problems Related to Recovery Systems and Other Fabric Structures. Proceedings of the 7th International LS-Dyna Users Conference, Dearborn MI, May 19-21, 2002.
8. Guide for the Verification and Validation of Computational Fluid Dynamics Simulations. AIAA Publication AIAA G-077-1998, 1998, Reston VA.
9. NASA Standard for Models and Simulations. NASA Publication NASA-STD-7009, 2006.
10. Sandia National Laboratories Predictive Capability Maturity Model for Computational Modeling and Simulation. Sandia Publication SAND-2007-5948, 2007.
11. Horta, L. G., Reaves, M. C., Jackson, K. E., Annett, M. S. Littell, J. D.: Fuselage Impact Testing and Simulation: A Model Calibration Exercise. Proceedings of the IMAC-XXII A Conference and Exposition on Structural Dynamics, Orlando FL, February 2014.
12. Lyle, K. H.: Preliminary Structural Sensitivity Study of Hypersonic Inflatable Aerodynamic Decelerator Using Probabilistic Methods. NASA TM-2014-218290, July 2014.
13. Jones, T. C.: Structural Certification of Human-Related Inflatable Space Structures. 2018 IEEE Aerospace Conference, 3-10 March 2018, Big Sky MT.

14. Doggett, W. R., Jones, T. C., Watson, J. J., Warren, J. E., Makino, A., Selig, M., and Mikulas, M. M., "Non-Axisymmetric Inflatable Pressure Structure (NAIPS) Concept that Enables Mass Efficient Packageable Pressure Vessels with Openings," 3rd AIAA Spacecraft Structures Conference, 2016 AIAA SciTech Forum and Exposition, AIAA Paper 2016-1475.
15. Jones, T. C., Doggett, W. R., Warren, J. E., Watson, J. J., Shariff, K. I., Makino, A., and Yount, B. C.: Non-Axisymmetric Inflatable Pressure Structure (NAIPS) Full-Scale Pressure Test. 4th AIAA Spacecraft Structures Conference/AIAA SciTech Forum, AIAA Paper 2017-0854, 9-13 January 2017, Grapevine TX.
16. Lyle, K. H. and Jones, T. C.: Demonstration of Probabilistic Sensitivity Analyses Tools on the Structural Response of a Representative Inflatable Space Structure. NASA TM-2018-219826, April 2018.
17. Lyle, K. H. and Jones, T. C.: Probabilistic Sensitivity Analyses Incorporating Surrogate Models Tools for the Structural Response of a Representative Inflatable Space Structure. NASA TM-2018-220082, August 2018.
18. *LS-Dyna Keyword User's Manual*, Version 971, July 27, 2012 (revision: 1617).
19. *LS-Opt User's Manual*, Version 5, December 2015.
20. Matlab Release 2015b, The MathWorks, Inc., Natick, Massachusetts, United States.
21. Halton, J.H.: On the Efficiency of Certain Quasi-Random Sequences of Points in Evaluating Multi-Dimensional Integrals. *Numerische Mathematik*, Vol. 2, 1960, pp. 84–90.
22. Montgomery, D. C.: *Design and Analysis of Experiments*. 6th Edition, John Wiley and Sons, 2005.
23. [Kriging] Sacks, J., Schiller, S. B., and Welch, W. J.: Design of Computer Experiments. Technometrics, Vol 31, No 1, 1989.
24. Saltelli, A.; Chan, K.; Scott, E. M.: *Sensitivity Analysis*. Chichester, England: John Wiley and Sons, 2000
25. Helton, J. C. and Davis, F. J.: Illustration of Sampling-Based Methods for Uncertainty and Sensitivity Analysis, *Risk Analysis*, Vol 22, No. 3, 2002 pp 591-622.
26. Sobol, I. M., *et al*: Estimating Approximation Error When Fixing Unessential Factors in Global Sensitivity Analysls. *Reliability Engineering and Safety*, Vol. 92, 2007, pp. 957-960.
27. Iooss B., Lemaître P. (2015) A Review on Global Sensitivity Analysis Methods. In: Dellino G., Meloni C. (eds) Uncertainty Management in Simulation-Optimization of Complex Systems. Operations Research/Computer Science Interfaces Series, vol 59. Springer, Boston, MA

Table I. Parameters for finite element simulations.

Parameter		FEM Execution Bounds		78 Stable Solutions		
		Lower	Upper	Minimum	Maximum	Mean
Factors applied to nonlinear stress-strain curves	F_{RC}	1.5	3.0	1.52	2.99	2.18
	F_{AC}	1.5	3.0	1.53	2.97	2.23
	F_{DF}	1.5	2.75	1.52	2.66	2.07
	F_{MF}	1.5	2.75	1.51	2.73	2.10
Friction values	μ_D	0.01	0.1	0.0114	0.0996	0.0550
	μ_M	0.01	0.1	0.0115	0.0990	0.0573
Cord thermal coefficients	α_{RC}	0.0015	0.0025	0.00151	0.00249	0.00197
	α_{AC}	0.0009	0.0013	0.000901	0.00130	0.00108

Table II. RMS Surrogate errors

Response	SM_1^+	SM_3
L_{RC}	~0	0.0398 (0.04%)
L_{AC}	~0	0.0517 (0.01%)
P_{RC}^5, lb	17.83 (0.87%)	17.4 (0.85 %)
P_{AC}^2, lb	118.9 (0.79%)	118.1 (0.78 %)
ε_{DF}^1, in/in	0.000319 (2.56 %)	0.000187 (1.49 %)
ε_{MF}^4, in/in	0.000164 (1.47%)	0.000120 (1.08 %)

Table III. Constraints and objectives

106.5 in **<** L_{RC} **<** 107.5 in

38.0 in **<** L_{AC} **<** 40.5 in

P_{RC}^5 **=** 2163 lb

P_{AC}^2 **=** 16,700 lb

ε_{DF}^1 = 0.0092 in/in

ε_{MF}^4 **=** 0.0092 in/in

Table IV. Calibration solutions.

Solution	Surrogate model		Optimization method	
	Linear + Crossterms (SM_1^+)	Kriging (SM_3)	Simulated Annealing (SA)	Genetic Algorithm (GA)
1	✓		✓	
2		✓	✓	
3	✓			✓
4		✓		✓

Table V. Calibration parameters.

Parameter		Bounds		Solutions			
		Lower	Upper	1	2	3	4
Factors applied to nonlinear stress-strain curves	F_{RC}	1.5	**4.0**	1.74	1.62	3.21	2.51
	F_{AC}	1.5	**4.0**	1.67	3.55	2.03	3.54
	F_{DF}	1.5	**3.1**	2.61	2.64	2.70	2.60
	F_{MF}	1.5	**3.1**	2.33	2.67	2.57	2.66
Friction values	μ_D	**0.0**	0.1	0.08	0.024	0.036	0.089
	μ_M	**0.0**	0.1	0.08	0.032	0.003	0.051
Cord thermal coefficients	α_{RC}	0.0015	**0.0030**	0.00204	0.00223	0.00196	0.00201
	α_{AC}	0.0009	**0.0020**	0.00180	0.00177	0.00139	0.00179

Table VI. Surrogate and FEM responses at calibration solutions.

Response	Solution 1		Solution 2		Solution 3		Solution 4	
	Surrogate	FEM	Surrogate	FEM	Surrogate	FEM	Surrogate	FEM
L_{RC}	107.4	106.9	107.1	106.7	107.4	107.0	107.4	107.0
L_{AC}	38.16	38.24	38.24	38.33	39.06	39.11	38.2	38.3
P_{RC}	2163	2077	2163	2098	2163	2078	2163	2086
P_{AC}	16,700	15,635	16,700	15,753	15,750	15,253	16,700	15,697
ε_{DF}	0.0092	0.0099	0.0092	0.0096	0.0092	0.0104	0.0092	0.0096
ε_{MF}	0.0092	0.0102	0.0092	0.0095	0.0092	0.0096	0.0092	0.0090
$Error_{RMS}$, %	5.91		3.49		5.45		3.58	

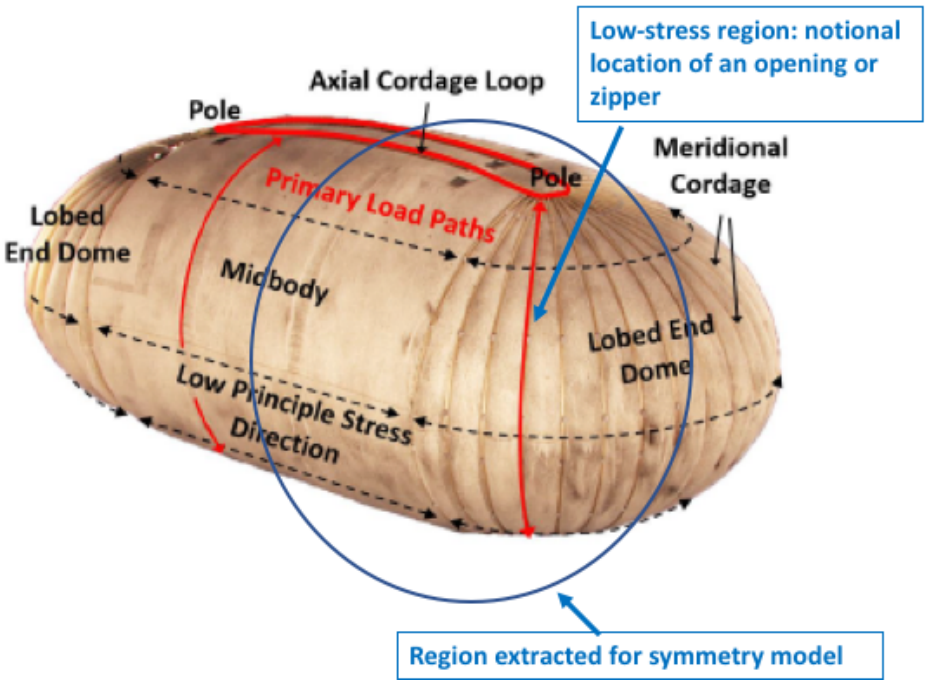

Figure 1. Photograph of inflated NAIPS test article[15].

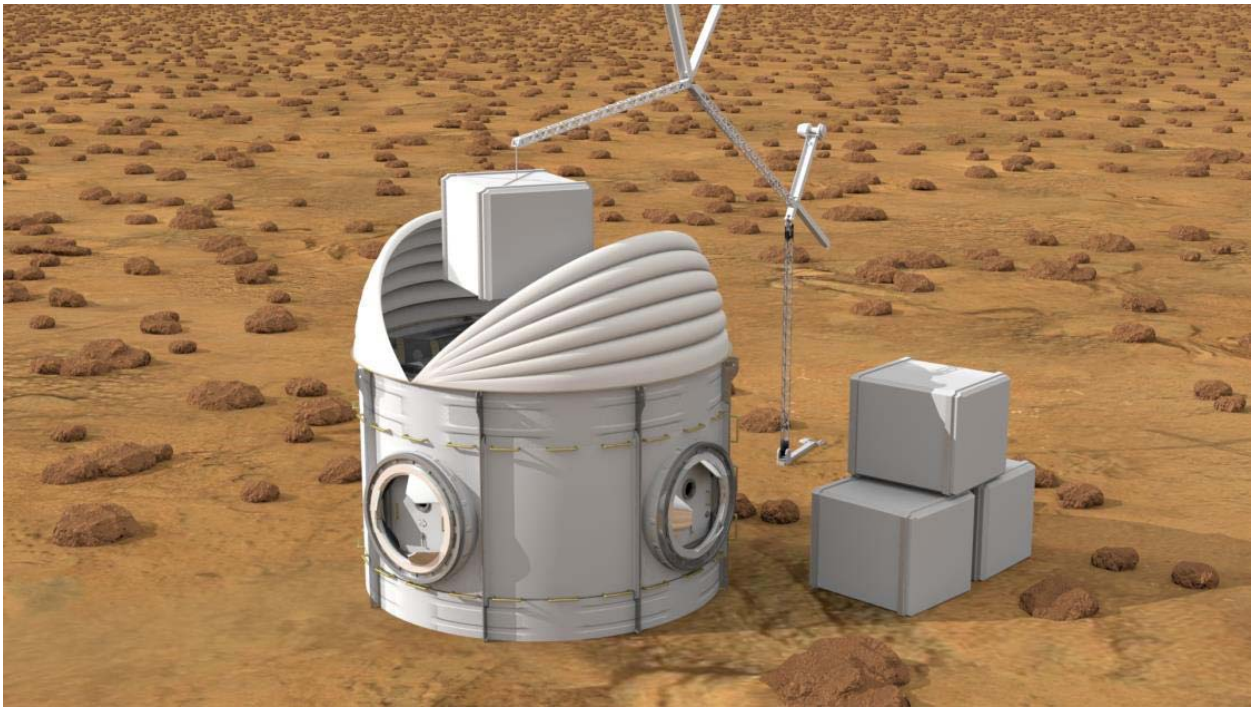

Figure 2. Large inflatable logistics bay on a Mars surface habitat.

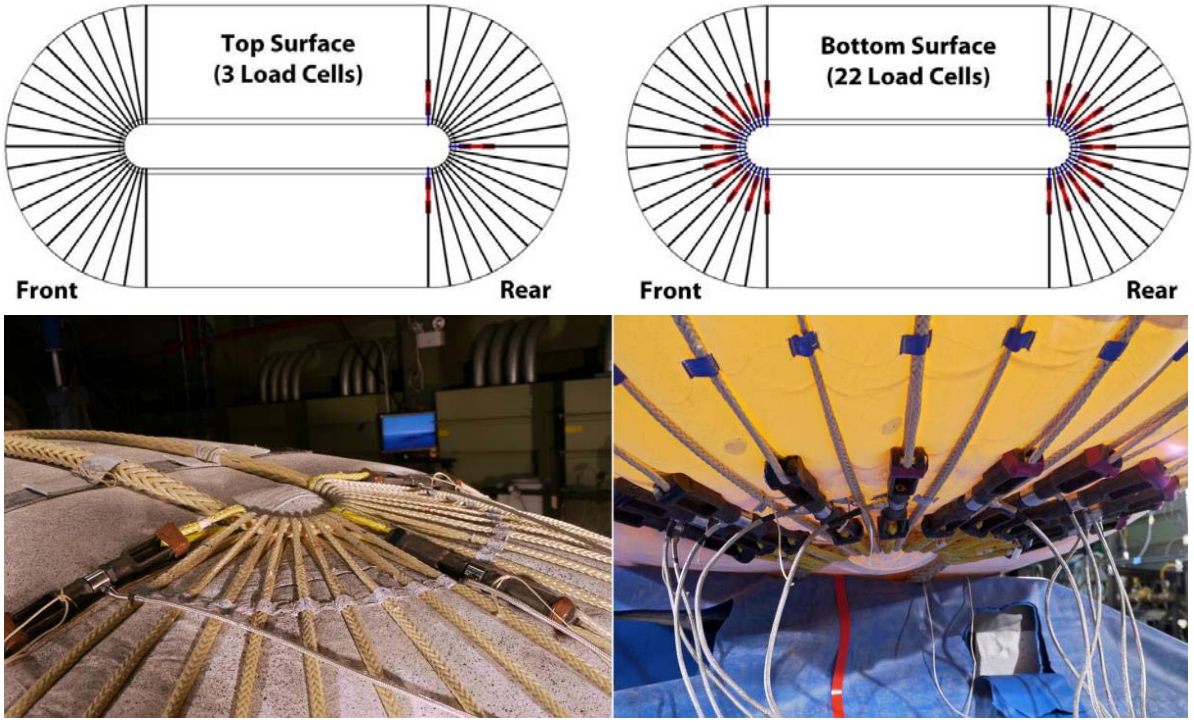

Figure 3. NAIPS full-scale test load cell configuration.

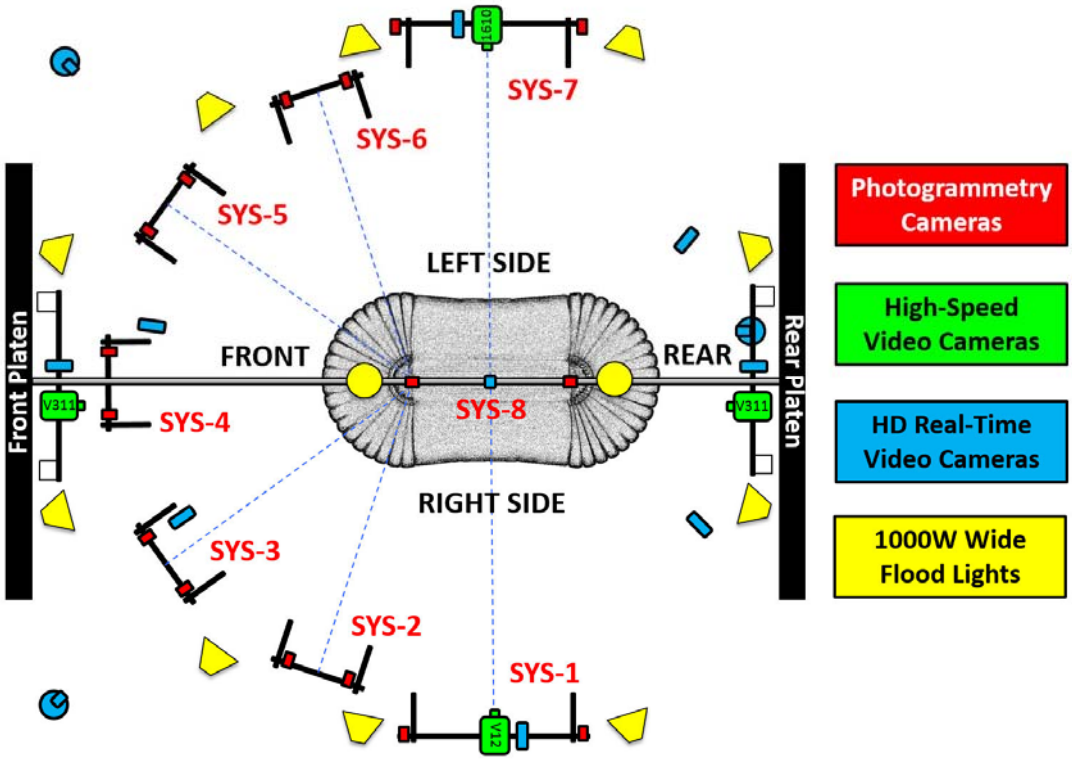

Figure 4. NAIPS photogrammetry strain measurement system setup.

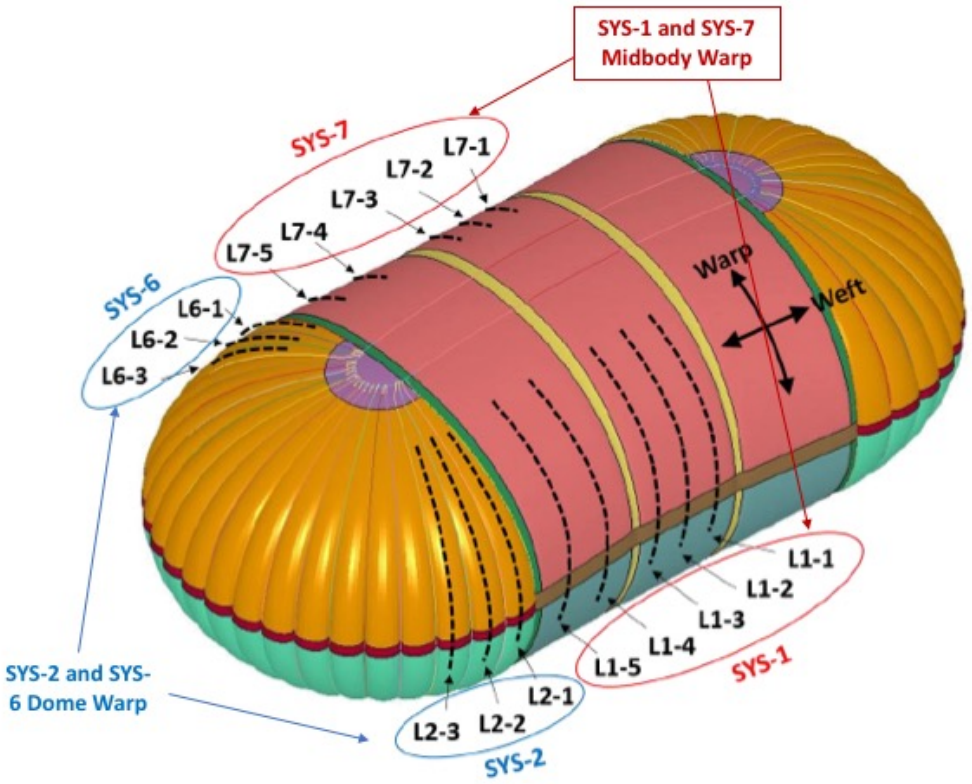

Figure 5. Schematic of dome FEM (D=displacement and R=rotation).

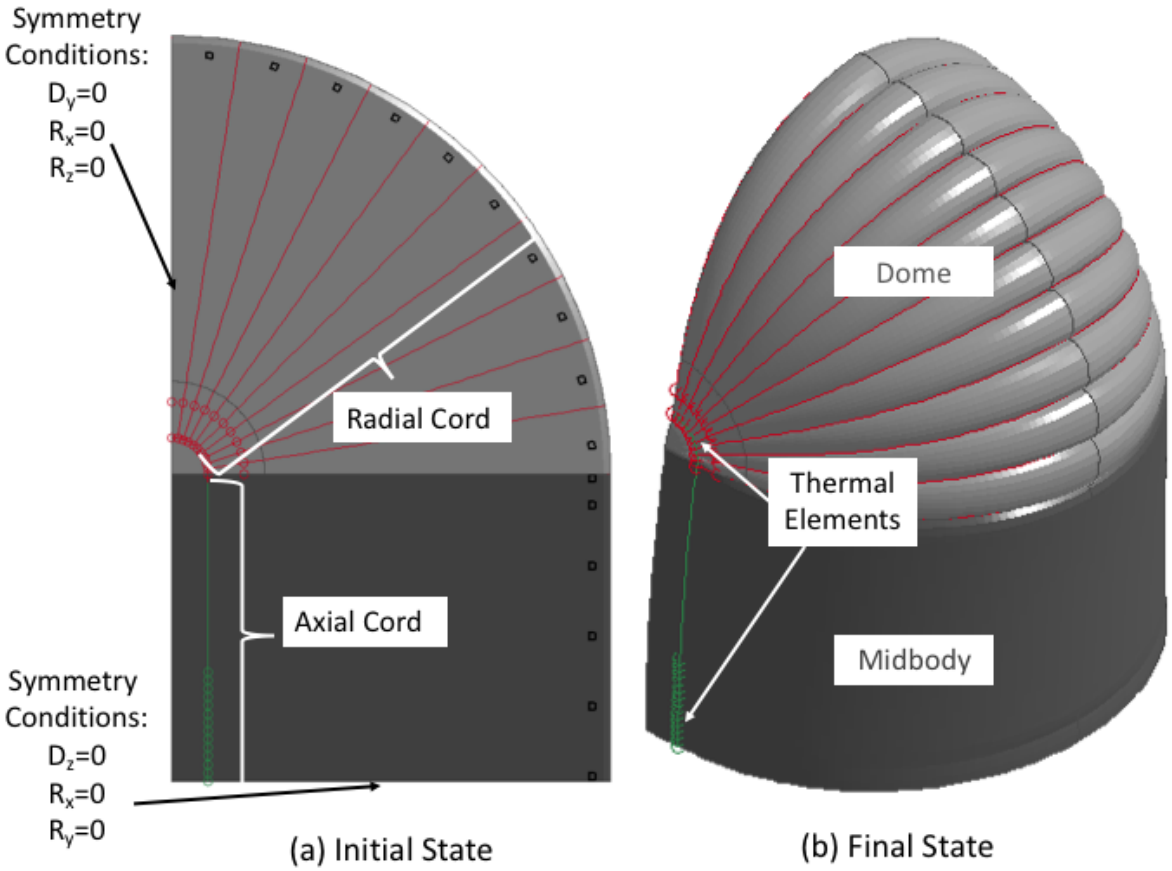

Figure 6. Schematic of dome FEM (D=displacement and R=rotation).

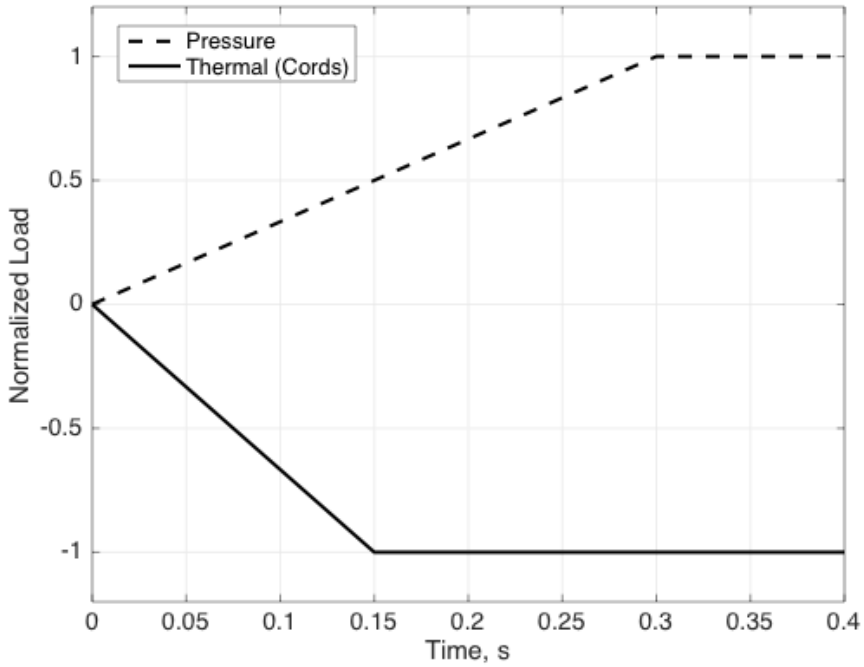

Figure 7. Non-dimensional loading profiles.

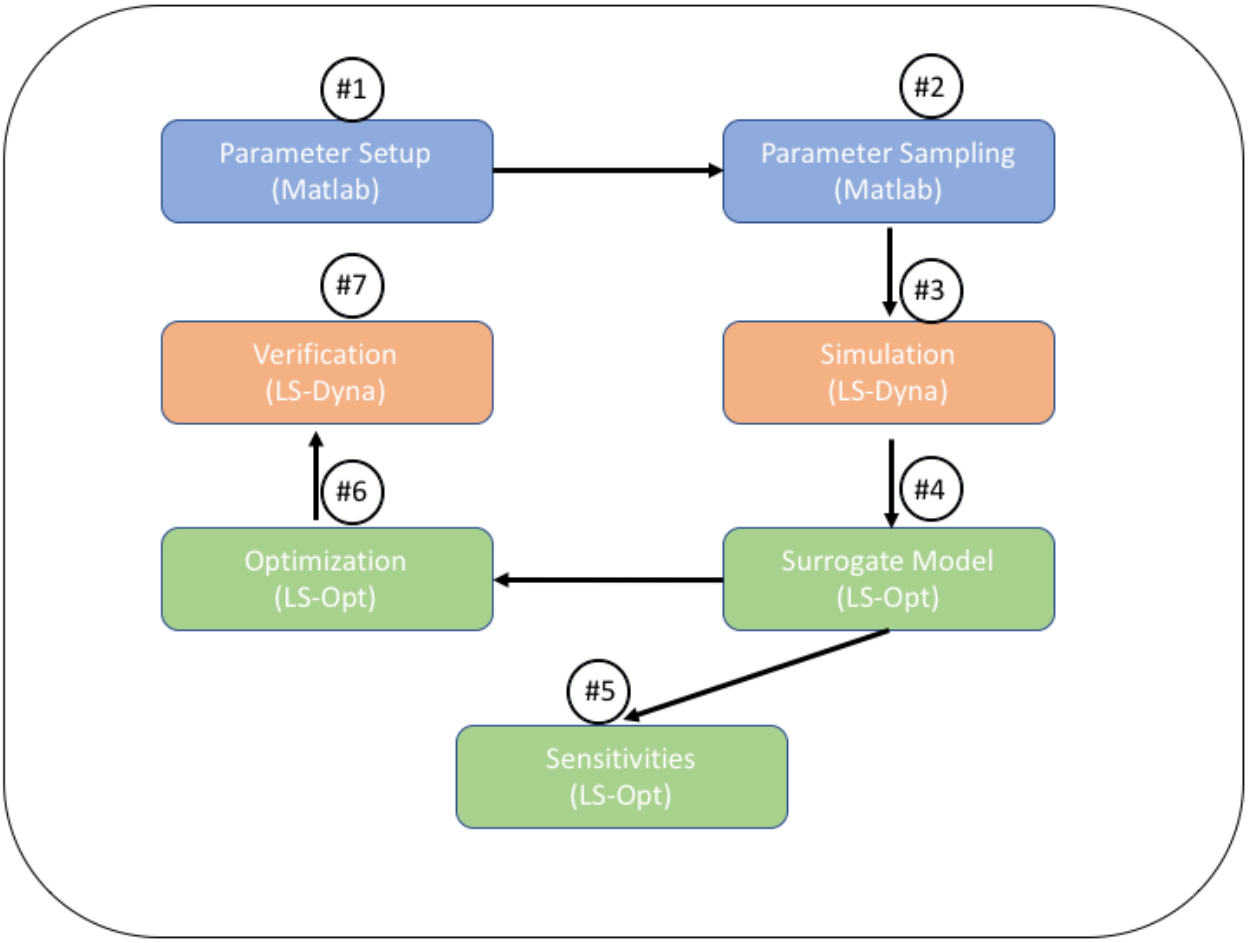

Figure 8. Model calibration flowchart.

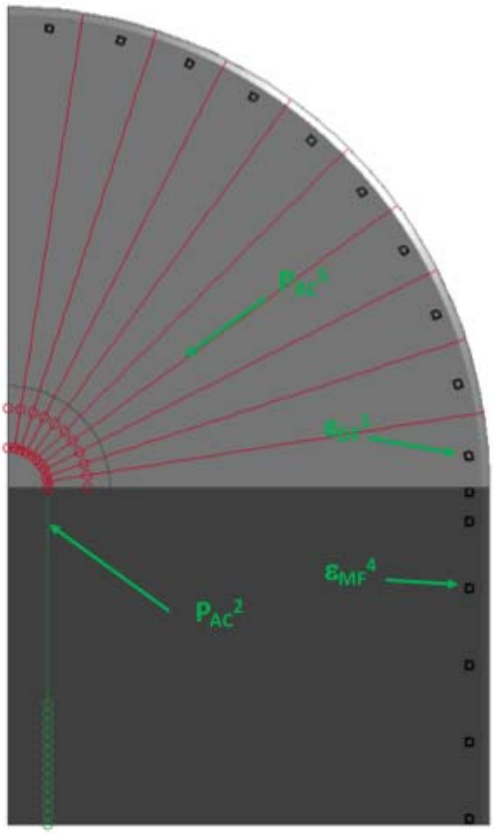

Figure 9. Responses for calibration.

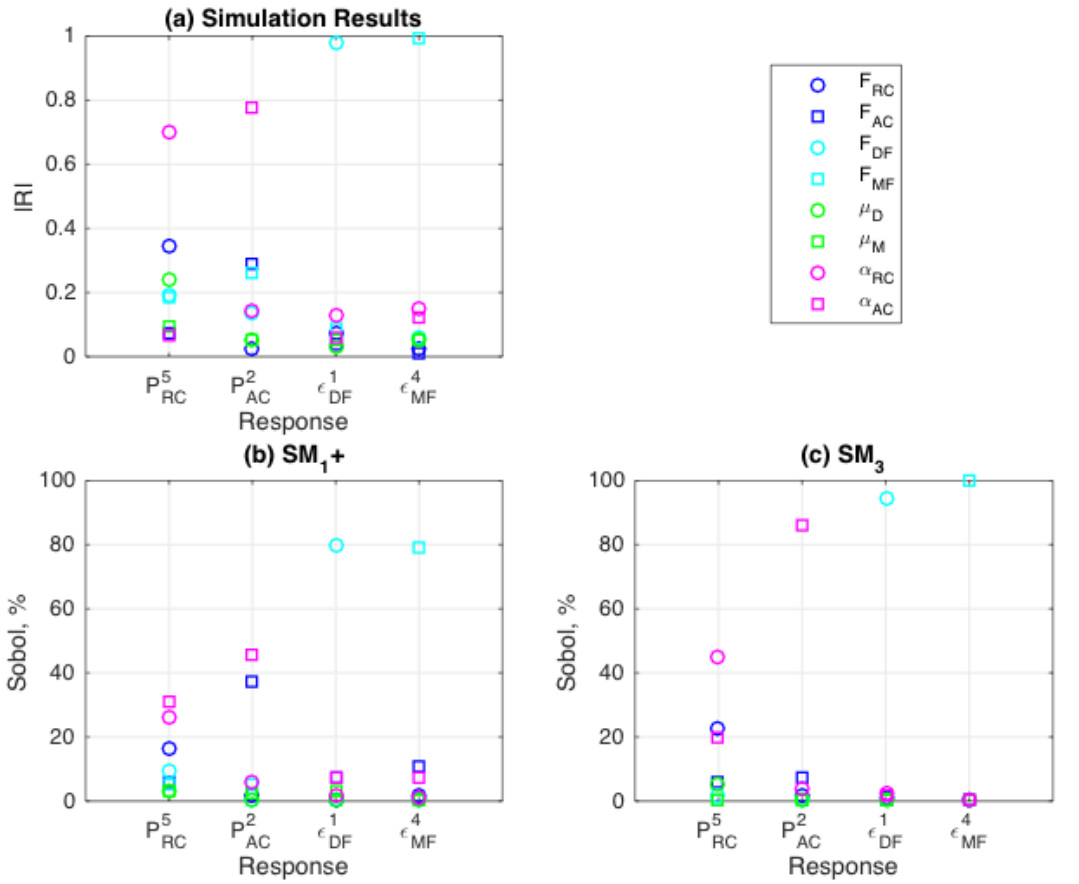

Figure 10. Sensitivity results.

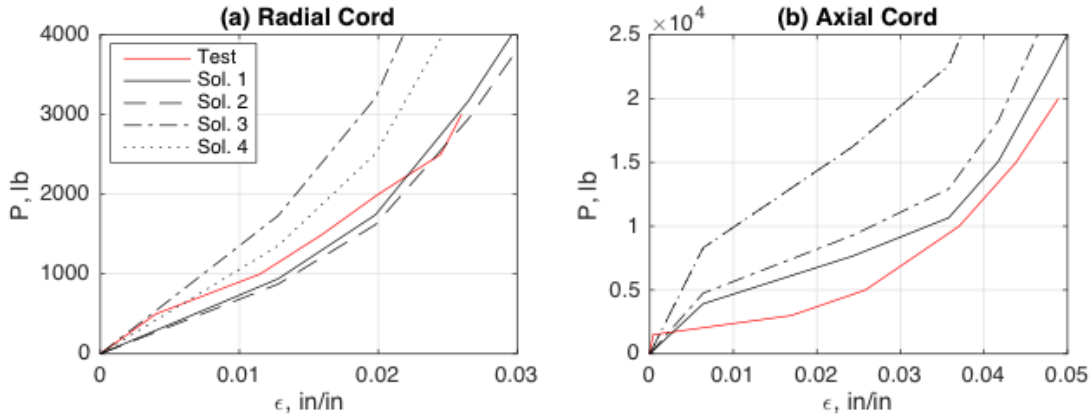

Figure 11. Cord nonlinear load-strain curves.

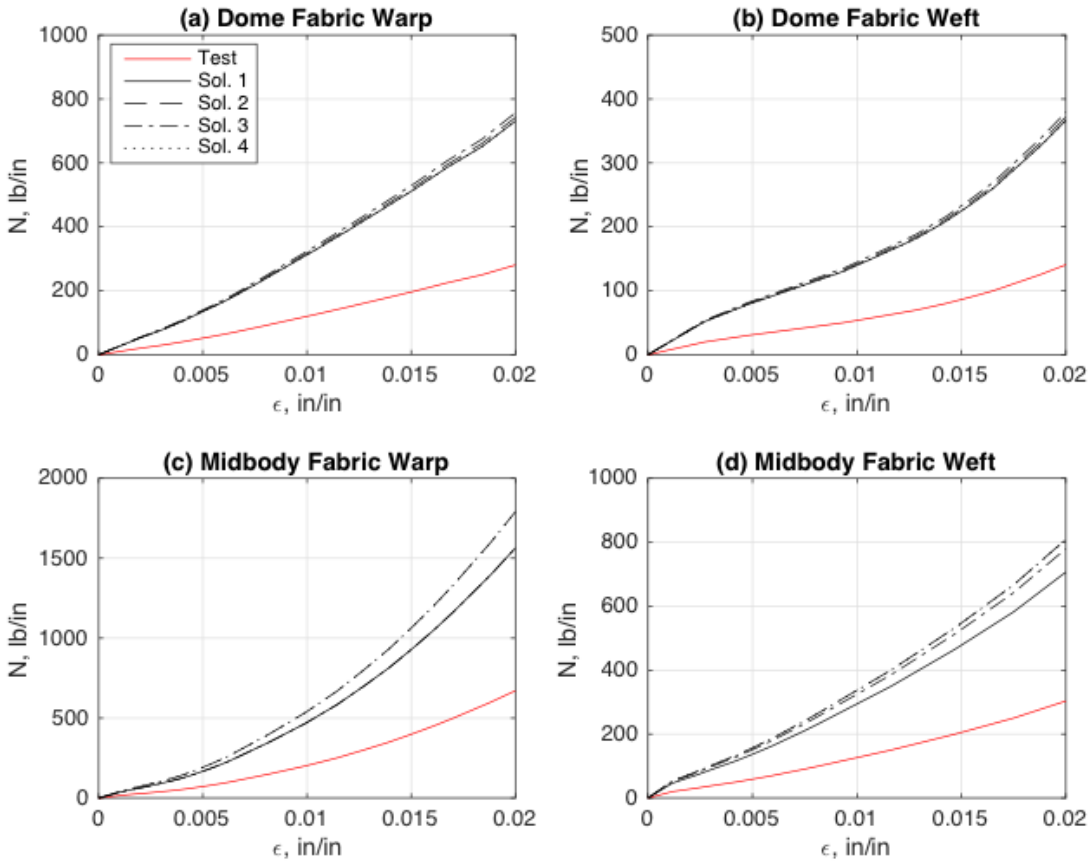

Figure 12. Fabric nonlinear line-load vs strain curves.

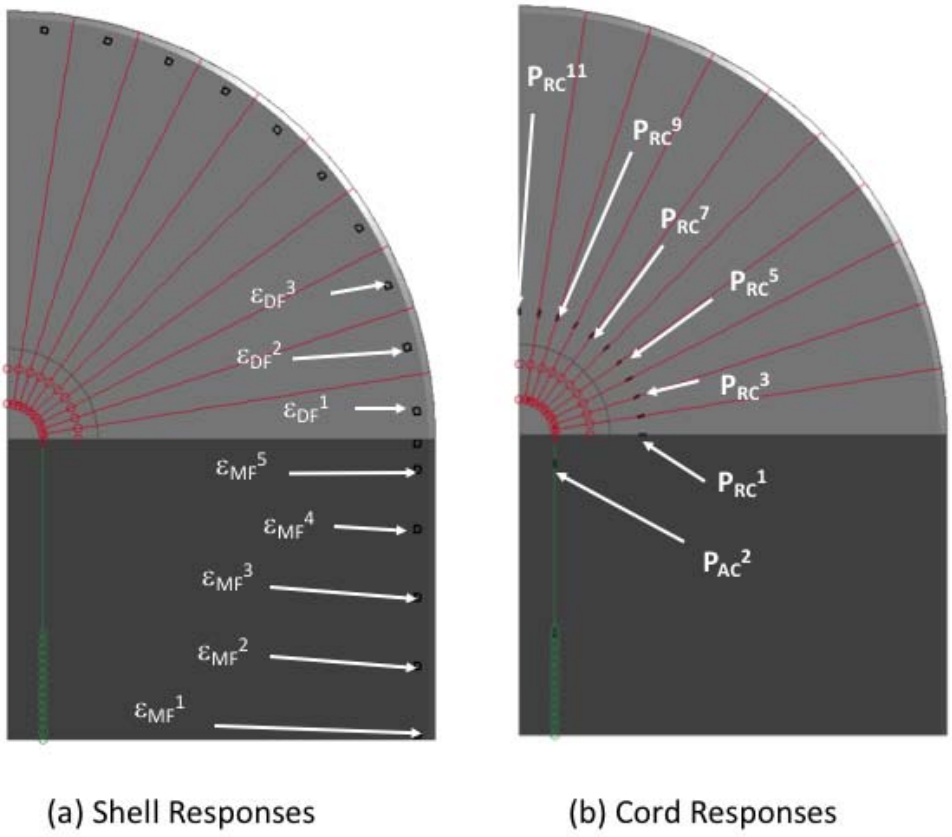

Figure 13. Schematic of expanded responses for comparison with test data.

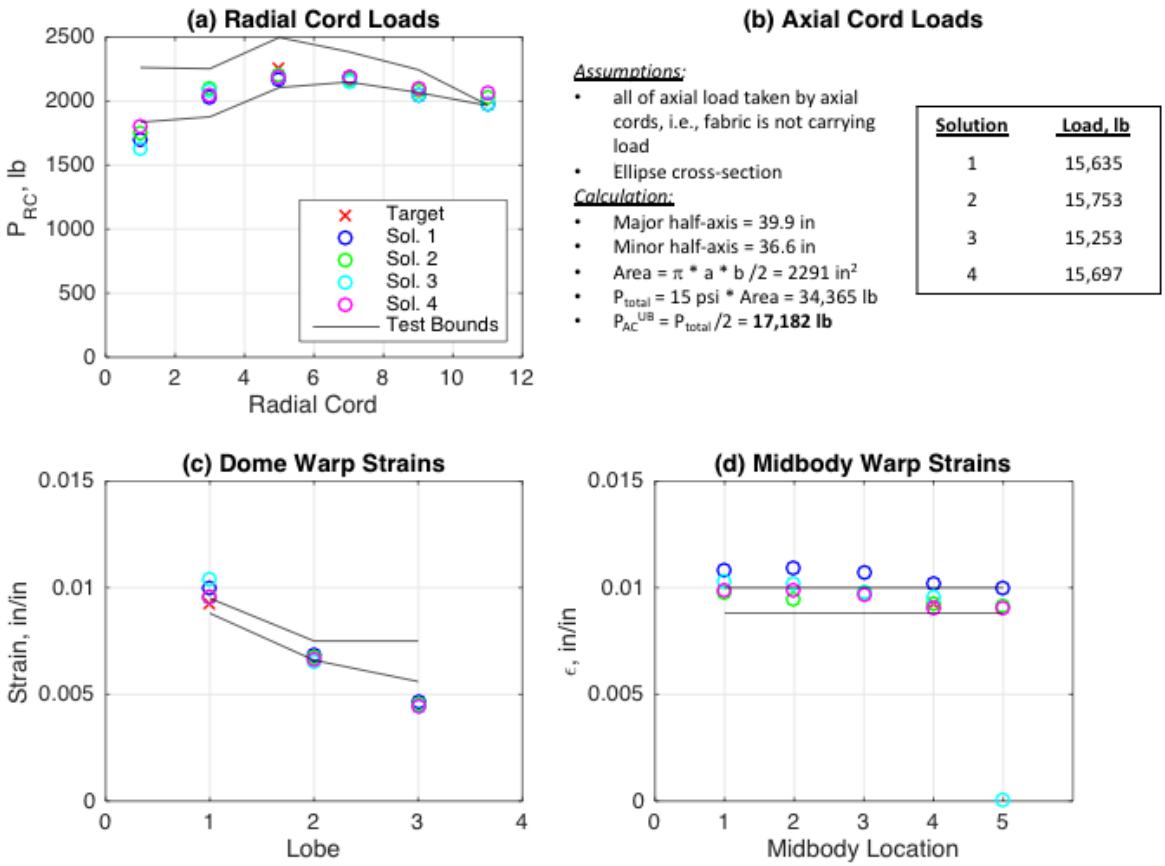

Figure 14. Effect of Solution on test vs analysis for 15 psi inflation pressure.

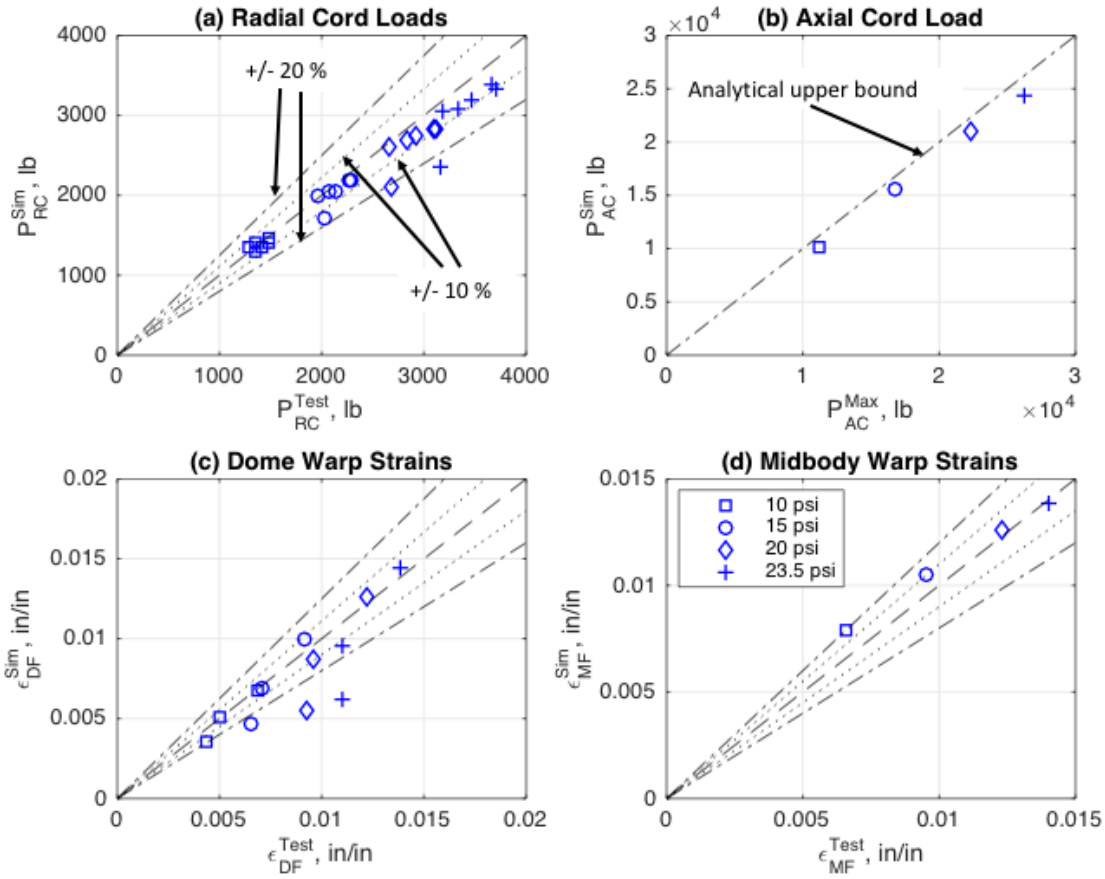

Figure 15. Effect of pressure on test vs analysis for Solution 1.

Appendix

The purpose of this appendix is to compare the modeling approaches used for the preliminary analyses of the MASH test article in Ref. 15 with the approaches used for the current calibration effort. A summary of test-analysis comparisons will be provided for the two modeling approaches followed by a description of the modeling modifications, which can be divided into three general categories: simplifications to reduce the number of uncertain parameters and the computation time; changes in modeling approach to mitigate numerical instabilities; and finally, changes in design parameters and approaches that significantly influence the numerical results.

Section VII.B of Ref. 15 lists 4 aspects to be evaluated, which were suggested could improve comparisons of the numerical results with the full-scale test data. They are paraphrased here: 1) include a technique to shorten the radial cords to the test lengths in the numerical model; 2) set the radial cord length based on the as-fabricated length, rather than adjusting the axial cord length to drive the radial cords to the measured loads; 3) improve numerical stability so all practical structural components (such as the seams) can be included; and 4) re-examine measured material property data for adequacy. The studies conducted to support the calibration effort directly addressed items 1, 2 and 4. The calibration effort did address numerical stability concerns, item 3, but was not focused on the responses at the seams as no test data were available. However, inclusion of the seam elements would be critical for detailed design studies and certification support. The radial cord loads were strongly dependent on the length, item 2. However, it was necessary to allow the cord lengths to vary within reasonable constraints to enable model calibration.

Comparisons of previous and current numerical results with full-scale test data

Results for the two modeling approaches are provided for the radial cord loads, dome fabric warp strains and midbody fabric warp strains in Figures A-1 to A-3. The comparisons are presented with the preliminary model comparisons (extracted from Ref. 15) on the left and the calibration model comparisons (see Figure 15) on the right. For each plot, the full-scale test data (on the x-axis) is compared with the numerical results (on the y-axis) for multiple inflation pressures. For reference, +/- 10% and +/- 20% error lines are plotted alongside the ideal 1:1 line, where the numerical result would exactly match the test data. The RMS error between test and simulation has been included on each plot.

For the radial cord loads, Figure A-1, the numerical results for the preliminary model under-predict the test data in all cases. Cord 1 is under-predicted by more than 50%. The calibrated model results on the right fall within +/- 10% of the test data for 88% of the points. Only the predictions for Cord 1 fall outside these error bounds, but are near the -20% bound. Incorporation of thermal elements to shorten these cords enables the calibration model to approach the test data, such that RMS error improves from 31 % to 9%.

Looking at the dome fabric strains in the warp direction, Figure A-2, the preliminary model

significantly over-predicted the strains by more than a factor of 2. The calibrated model predicts the measured responses to with +/-10 % for 58% of the samples, with particular issues related to Lobe 3. Focusing in more detail on 15 psi, the calibrated model strains in the warp and radial directions for the three lobes along with the test data are provided in Table A-1. These results show that a small change in measurement direction (or alignment) for Lobe 3 could significantly change the measured strains. More specifically, if the line used for measuring strains was not perfectly aligned with the fabric warp direction, but migrated toward the lobe radial direction, then the "measured" strains could be lower. Two factors contributed to the significant improvement in comparisons for the calibrated model (i.e., RMS error reduced from 278% to 21%): the radial cords in the calibrated model are taking more load, thus helping to offload the fabric; and the fabric material property curves were calibrated to a more realistic stiffness versus the prior material model.

For the midbody fabric strains in the warp direction, Figure A-3, the preliminary model consistently over-predicted the strains, by more than 20%. The calibrated model predicted 75% of the strains within 10% of the test data and overall the RMS error was reduced from 65% to 11%. The primary contributor to the change between the preliminary and calibrated results is the stiffer stress-strain material properties assigned to the fabric. It is interesting to note in Table V that the factors for the fabric for all of the solutions ranged from 2.33 to 2.70. As has been previously noted, this is a strong indicator that the measurement method to determine the underlying fabric material properties needs to be re-examined.

Significant modeling modifications

Model simplifications

It was important to simplify the model for a number of reasons. Shortening the computation time enabled hundreds of analysis runs to be executed, which supported a rapid evaluation of modeling changes and subsequently enabled implementation of probabilistic methods. The improved understanding of the key parameters driving the model variations enabled the elimination of second-order effects and detailed model components, such as seams and radial cord loops. Shortening the computation time was accomplished by focusing on a quarter-symmetry model and calibrating to a single inflation pressure of 15 psi, the operational pressure. The initial simplifications, as reported in Refs. 16 and 17, first focused on a quarter-symmetry section of the dome only. Once the dome-only model was considered sufficiently mature, the midbody was added for the current report and comparison.

The effect of seaming was assessed through a series of simulations that changed the material properties of a corresponding strip of the model along the midbody seam line. The primary impact of the seam at the dome-midbody interface was on Cord 1 (which lay at the interface). The effect on the other cord loads of the seam property changes was insignificant. The Cord 1 loads were strongly related to the ratio of the stiffnesses of the dome and midbody fabrics.

Essentially, the Cord 1 response could be tuned using additional parameters, in addition to the primary parameters important to the other responses.

Numerical stability

To incorporate probabilistic methods, support design studies and expand confidence in predictive capability, it was important to improve the numerical stability of the simulations. Two modeling areas were identified as the primary sources that produced numerical instability. These were: 1) the scale factor applied to the contact forces between softgoods elements; and 2) the convergence of 80 triangular elements at the poles of the dome. It was possible with the current model to mitigate the contact force induced instabilities by simply reducing the factor between the radial cords and the dome fabric from the default of 1.0 to 0.1 or even 0.01. These factors are in effect during the entire simulation. They control the amplitude of the force that is applied to a node to push it away once it has penetrated a surface. The force is based in part on the relative stiffnesses of the two contacting parts. LS-Dyna has a "soft" option (which was selected for the current application) in the contact which is designed to help with two contacting parts that have a wide difference in elastic bulk moduli. The "soft" contact can mitigate some issues, but it can also end up with a higher contact stiffness. In the end, the point of the contact is to keep the two parts from penetrating, without pushing the parts away in a nonphysical manner. It was found that reducing this factor changed the resulting radial cord loads by less than 1 percent. There was not enough time during these current studies to re-mesh the dome center section, which would be an area to address for any follow-on efforts. The instabilities arising from the mesh at the poles of the dome were particularly problematic when the midbody was included and the axial cords were contracted.

Model modifications

In addition to removing some of the 2nd-order effects, identified in the simplification section, the following major changes were made to the overall model. Thermal elements were included in the radial cords to shrink them to the as-fabricated and tested lengths. For example, shrinking the radial cords 2" can increase the cord loads by 400 lb. In addition, during the actual test, load cells with pin-clevis attachments (approximately 12" in total length) were used in many of the cords, thus 12"-long stiff elements were tested in the model and shown to increase the radial cord loads by 100 lbs. For this reason, 100 lbs. was added to the simulation radial cord load values.

The second significant modification was related to the material properties. The fabric strain responses were dominated by changes in material stress-strain properties. For the calibration studies, the properties were allowed to vary by a factor up to 3.1. Looking at the midbody warp fabric strain as an illustrative example, a simple analysis for the midbody warp strains is provided in Figure A-4. This analysis confirms that the measured fabric properties are

not stiff enough to produce the full-scale strain measurements.

Table A-1. Dome lobe strains at 15 psi for Solution 1

Lobe	Radial, in/in	Warp, in/in	Test, in/in
1	0.0104	0.0099	0.0092
2	0.0121	0.0068	0.0070
3	0.0143	0.0046	0.0066

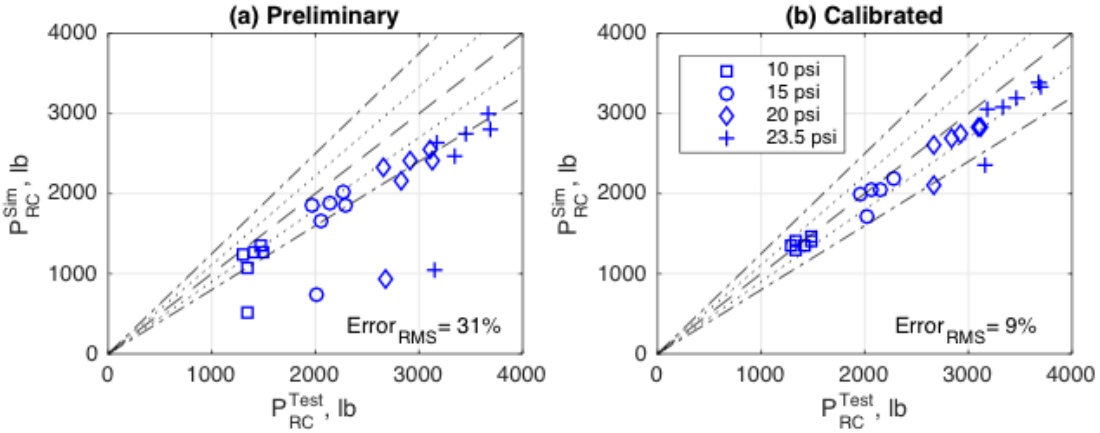

Figure A-1. Radial cord loads: test vs analysis for preliminary and calibrated models.

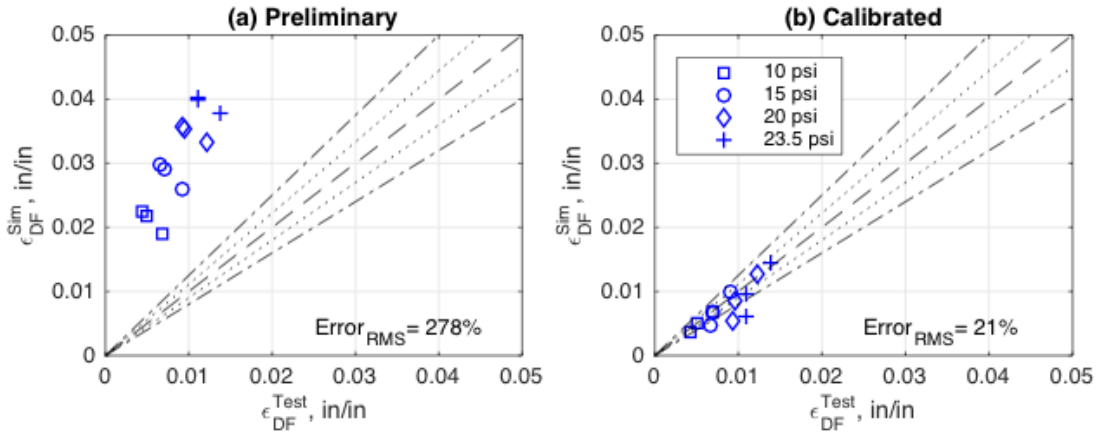

Figure A-2. Dome fabric warp strains: test vs analysis for preliminary and calibrated models.

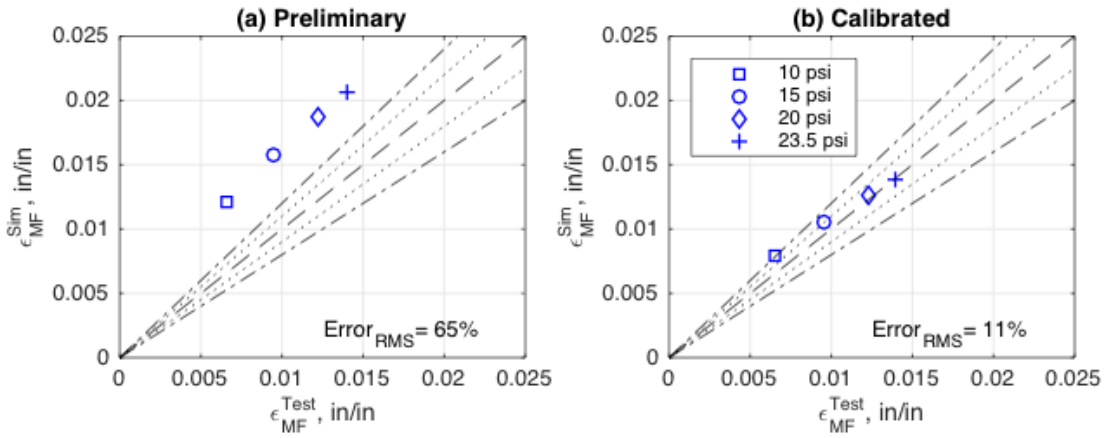

Figure A-3. Midbody fabric warp strains: test vs analysis for preliminary and calibrated models.

Thin-walled cylinder hoop stresses:

Given:

- Pressure = 15 psi
- Thickness (t) = 0.024 in
- Radius (R) = 38.2 in

[Circumference (C) = 240 in; C = 2πR]

Response:

- σ_{Hoop} = Pressure * R / t = 23,875 lb/in^2
- N_{Hoop} = σ_{Hoop} * t = 573 lb/in

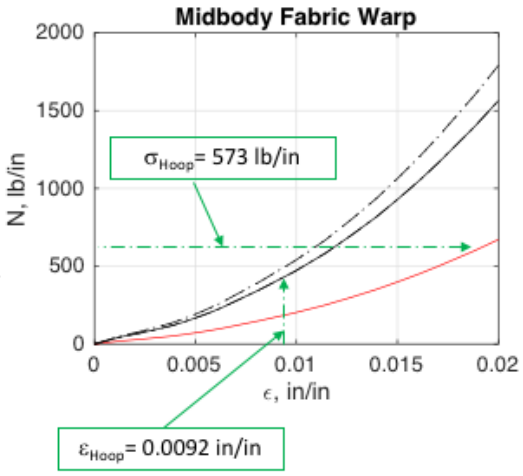

Figure A-4. Analysis of midbody warp strains.

REPORT DOCUMENTATION PAGE

Form Approved
OMB No. 0704-0188

1. REPORT DATE *(DD-MM-YYYY)*
1-02-2019

2. REPORT TYPE
Technical Memorandum

3. DATES COVERED *(From - To)*

4. TITLE AND SUBTITLE

Calibration of a Structural Finite Element Model for a Representative Inflatable Space Structure Utilizing Probabilistic Methods and Surrogate Models

5a. CONTRACT NUMBER

5b. GRANT NUMBER

5c. PROGRAM ELEMENT NUMBER

6. AUTHOR(S)

Lyle, Karen H.; Jones, Thomas C..

5d. PROJECT NUMBER

5e. TASK NUMBER

5f. WORK UNIT NUMBER
08947.01.23

7. PERFORMING ORGANIZATION NAME(S) AND ADDRESS(ES)

NASA Langley Research Center
Hampton, VA 23681-2199

8. PERFORMING ORGANIZATION REPORT NUMBER
L-20996

9. SPONSORING/MONITORING AGENCY NAME(S) AND ADDRESS(ES)

National Aeronautics and Space Administration
Washington, DC 20546-0001

10. SPONSOR/MONITOR'S ACRONYM(S)
NASA

11. SPONSOR/MONITOR'S REPORT NUMBER(S)
NASA-TM-2019-220250

12. DISTRIBUTION/AVAILABILITY STATEMENT

Unclassified-
Subject Category 39
Availability: NASA STI Program (757) 864-9658

13. SUPPLEMENTARY NOTES

14. ABSTRACT

A structural finite element model representing a novel inflatable airlock concept has been calibrated using full-scale test data. The concept, denoted as the Non-Axisymmetric Inflatable Pressure Structure (NAIPS), was developed under NASA's Minimalistic Advanced Softgoods Hatch (MASH) Program. The current studies extended previous numerical efforts by incorporating the midbody section of the NAIPS to the dome section and calibrating the model with test data using a process that included surrogate models. Brief overviews of the finite element model and calibration process are provided. The completion of the calibration process provided a model that adequately replicated the test data. The successful demonstration of calibration of a finite element model representing an inflatable habitat provides confidence in the ability to use numerical simulations and associated surrogate models to support design and certification of inflatable space habitats.

15. SUBJECT TERMS

Inflatable Space Structures; Model Calibration Surrogate Models; Softgoods; Structural Analysis

16. SECURITY CLASSIFICATION OF:			17. LIMITATION OF ABSTRACT	18. NUMBER OF PAGES	19a. NAME OF RESPONSIBLE PERSON
a. REPORT	b. ABSTRACT	c. THIS PAGE			STI Help Desk (email: help@sti.nasa.gov)
U	U	U	UU	34	19b. TELEPHONE NUMBER *(Include area code)* (757) 864-9658